Journal of Magnetism and Magnetic Materials 421 (2017) 138–151

Contents lists available at ScienceDirect

Journal of Magnetism and Magnetic Materials

journal homepage: www.elsevier.com/locate/jmmm

AC susceptibility as a tool to probe the dipolar interaction in magnetic nanoparticles

Gabriel T. Landi [a,*], Fabiana R. Arantes [a], Daniel R. Cornejo [b], Andris F. Bakuzis [c], Irene Andreu [d], Eva Natividad [d]

[a] Universidade Federal do ABC, 09210-580 Santo André, Brazil
[b] Instituto de Física da Universidade de São Paulo, São Paulo 05508-090, Brazil
[c] Instituto de Física, Universidade Federal de Goiás, 74690-900 Goiânia-GO, Brazil
[d] Instituto de Ciencia de Materiales de Aragón (ICMA), CSIC-Universidad de Zaragoza, Zaragoza 50018, Spain

ARTICLE INFO

Article history:
Received 11 April 2016
Received in revised form
19 June 2016
Accepted 2 August 2016
Available online 3 August 2016

Keywords:
AC susceptibility
Magnetic hyperthermia
Magnetic nanoparticles

ABSTRACT

The dipolar interaction is known to substantially affect the properties of magnetic nanoparticles. This is particularly important when the particles are kept in a fluid suspension or packed within nano-carriers. In addition to its usual long-range nature, in these cases the dipolar interaction may also induce the formation of clusters of particles, thereby strongly modifying their magnetic anisotropies. In this paper we show how AC susceptibility may be used to obtain information regarding the influence of the dipolar interaction in a sample. We develop a model which includes both aspects of the dipolar interaction and may be fitted directly to the susceptibility data. The usual long-range nature of the interaction is implemented using a mean-field approximation, whereas the particle-particle aggregation is modeled using a distribution of anisotropy constants. The model is then applied to two samples studied at different concentrations. One consists of spherical magnetite nanoparticles dispersed in oil and the other of cubic magnetite nanoparticles embedded on polymeric nanospheres. We also introduce a simple technique to address the presence of the dipolar interaction in a given sample, based on the height of the AC susceptibility peaks for different driving frequencies.

1. Introduction

Magnetic nanoparticles (MNPs) have been an active topic of research for over half a century. Initially, much of this interest was related to the magnetic recording industry, but in the past few decades there has been a shift toward biomedical applications [1]. Examples include the use of MNPs for drug delivery [2], stem cell labeling [3,4], contrast agents for nuclear magnetic resonance [5] and magnetic hyperthermia [6–15]. The latter, in particular, is a cancer treatment technique that has already entered clinical trials [15] and is now considered the most promising application of MNPs. Great progress has also been made in our theoretical understanding of MNPs, particularly through Brown's Fokker-Planck equation [16,17], which allows one to make valuable predictions about several dynamic properties [18–24].

Most of our theoretical understanding about MNPs concerns non-interacting samples. However, MNPs are also strongly influenced by the dipolar interaction [25–50]. Indeed, recent papers [10–12,42,43,50] have shown that the dipolar interaction has a strong influence in magnetic hyperthermia treatments. This means that the heating properties of particles diluted in a fluid will be very different from those of particles packed inside cells or nano-carriers, such as magnetoliposomes [12,51,52]. Hence, when tailoring a sample for a specific treatment, one must also take into account the spatial arrangement of the nanoparticles. Recently, several theoretical models [10,25,42,43] and simulations methods [50] have been developed to deal with the dipolar interaction and aid in the design of samples for specific treatments.

However, in samples where the particles have some degree of mobility, as is true for many samples used for hyperthermia, the dipolar interaction may also induce the formation of aggregates (sometimes observed in the form of elongated chains [10,53]). The strong interaction between particles within a cluster cause them to rotate in order to align their easy axes, therefore modifying their effective magnetic anisotropy [10,54]. Despite its importance, this effect is seldom taken into account when developing theoretical models.

The modifications in the effective magnetic anisotropy of a given MNP will depend on the size and shape of the aggregate that it resides in, and also on the position and relative orientation of that

* Corresponding author.
E-mail address: gtlandi@gmail.com (G.T. Landi).

http://dx.doi.org/10.1016/j.jmmm.2016.08.011
0304-8853/

MNP within the cluster. Consequently, this effect may be modeled by considering a distribution of anisotropy constants, in addition to the distribution of volumes. The distribution of anisotropies already has an intrinsic, concentration-independent, contribution due to fluctuations in the crystallinity, shape and surface roughness. The contribution from particle–particle interactions should therefore enter as an additional effect, which may be small for diluted samples, but may very well be dominant when the particle aggregation is high.

Experimentally accessing and quantifying the degree of aggregation, however, is by no means trivial. This problem has generated much interest lately, with recent proposals involving the use of Lorentz microscopy [55] and small angle X ray scattering [56]. The purpose of this paper is to show that AC susceptibility also yields important information concerning the state of aggregation in a sample.

The most common analysis of AC susceptibility curves is the Arrhenius plot, which looks at the temperature $T_{\max}$ where the imaginary part χ'' is a maximum. A plot of $T_{\max}$ as a function of the frequency f of the AC field usually yields a straight line [cf. Eq. (5) to be discussed below], from which one may extract information about the average anisotropy energy barrier and the typical precession time τ_0 (whose values may be used to estimate the magnitude of the dipolar interaction [29]). Since one uses only the maximum of the imaginary curve, this analysis clearly underuses the data since from each χ'' vs. T dataset, just a single point is taken. Moreover, the effects of the particle size distribution only enter indirectly in the average anisotropy barrier. A more robust approach was introduced by Jonsson et. al. [57], who developed a model for χ'' that be fitted to the entire dataset, taking into account the size distribution.

In this paper we show how to expand on the model of Ref. [57] to include both aspects of the dipolar interaction. This is done using a mean-field approximation [42] to model the long-range effect, together with a anisotropy distribution to model the particle aggregation. This approach allows us to extract information which reflects the different levels of particle aggregation within the sample. We apply this model to two samples, a commercial magnetite-based ferrofluid dispersed in oil, and a sample containing PLGA [the poly(D,L-lactide-*co*-glycolic) acid copolymer] nanospheres with cubic nanoparticles trapped on their surface.

We also introduce a new very simple tool to access the qualitative importance of the dipolar interaction in a given sample. It is based on analyzing the maximum height $\chi''_{\max}$ of the χ'' vs. T curves as a function of the frequency f. When the dipolar interaction is negligible in a sample, $\chi''_{\max}$ should not increase with f. Conversely, we show that the presence of a dipolar interaction causes $\chi''_{\max}$ to *increase* with f. Hence, this serves as a signature of the dipolar interaction. Through a simple visual analysis of the imaginary AC susceptibility curves it is possible to see if the dipolar interaction is relevant in that given sample or not.

2. Theory

2.1. AC susceptibility for ideal monodisperse samples

We begin by reviewing the theory of AC susceptibility. The relaxation time of a single-domain magnetic nanoparticle with volume V and uniaxial anisotropy constant K is given approximately by the Néel formula [58]:

$$\tau \simeq \tau_0 e^{\sigma} \tag{1}$$

where $\tau_0 \sim 10^{-9}$ s and

$$\sigma = \frac{\theta}{T} = \frac{KV}{k_B T} \tag{2}$$

The quantity $\theta = KV/k_B$, which will be used throughout the text, represents the height of the energy barrier in temperature units. For more information, see supplemental information.

In AC susceptibility experiments one measures the response of a sample to an alternating magnetic field $H(t) = H_0 \cos\omega t$, of frequency $f = \omega/2\pi$ and very low amplitude H_0. From linear response theory (see Ref. [17] or the supplemental information) one finds that the real and imaginary part of the susceptibility are given by

$$\chi' = \chi_0 \frac{1}{1 + (\omega\tau)^2}, \qquad \chi'' = \chi_0 \frac{\omega\tau}{1 + (\omega\tau)^2} \tag{3}$$

where χ_0 is the static susceptibility. As will be discussed in Section 2.3, it is convenient to measure the response in terms of the magnetic moment instead of the magnetization. Consequently, the correct formula for χ_0 is

$$\chi_0 = \frac{(M_s V)^2}{3 k_B T} \tag{4}$$

In Fig. 1(a) we show examples of Eq. (3) for $\theta = 400$ K, $\tau_0 = 10^{-9}$ s and different frequencies f. The discrepancy between these curves and data usually reported in the literature is partly due to the fact that the size distribution is not yet included.

Experimental curves of χ'' vs. T are usually analyzed by looking at the temperature where χ'' is a maximum, $T_{\max}$. According to Eq. (3) the maximum occurs at $\omega\tau = 1$, which implies the equation

$$-\ln(2\pi f) = \ln(\tau_0) + \frac{\theta}{T_{\max}} \tag{5}$$

Hence, a plot of $-\ln(2\pi f)$ vs. $1/T_{\max}$ should yield a straight line, from which it is possible to extract τ_0 and θ. This analysis, usually referred to as an Arrhenius plot, clearly underuses the available information, since from the entire data set only a single point is used (the maximum). Moreover, it is also very sensitive to experimental uncertainties.

2.2. Samples with a size distribution

Next we include the effects of a size distribution. Let $P(D)$ denote the probability that a particle randomly drawn from the sample has diameter D (experimentally, $P(D)$ may be obtained from TEM measurements). It is customary to model $P(D)$ by a lognormal distribution

$$P(D) = \frac{1}{\sqrt{2\pi}\delta_D D} e^{-\frac{\ln^2(D/D_0)}{2\delta_D^2}} \tag{6}$$

with parameters D_0 and δ_D. The parameter D_0 in Eq. (6) is the median of $P(D)$ and not the average diameter, which reads $D_0 e^{\delta_D^2/2}$. Moreover, δ_D is a dimensionless parameter related to the standard deviation (SD) by $\mathrm{SD} = D_0 e^{\delta_D^2/2}\sqrt{e^{\delta_D^2} - 1}$. Defining the root-mean-square deviation as the ratio between the standard deviation and the mean diameter, we therefore get

$$\text{r. m. s.} = \sqrt{e^{\delta_D^2} - 1} \simeq \delta_D \tag{7}$$

Hence, δ_D is a measure of the root-mean-square deviation. Samples with $\delta_D \lesssim 0.1$ (10%) are usually considered monodisperse in the MNP synthesis literature.

From the distribution of diameters $P(D)$, we may also look at the distribution of volumes $P(V)$. For this purpose, the lognormal distribution turns out to be quite useful since, if D is lognormal, so will aD^k, with parameters aD_0^k and $|k|\delta_D$. This means that the

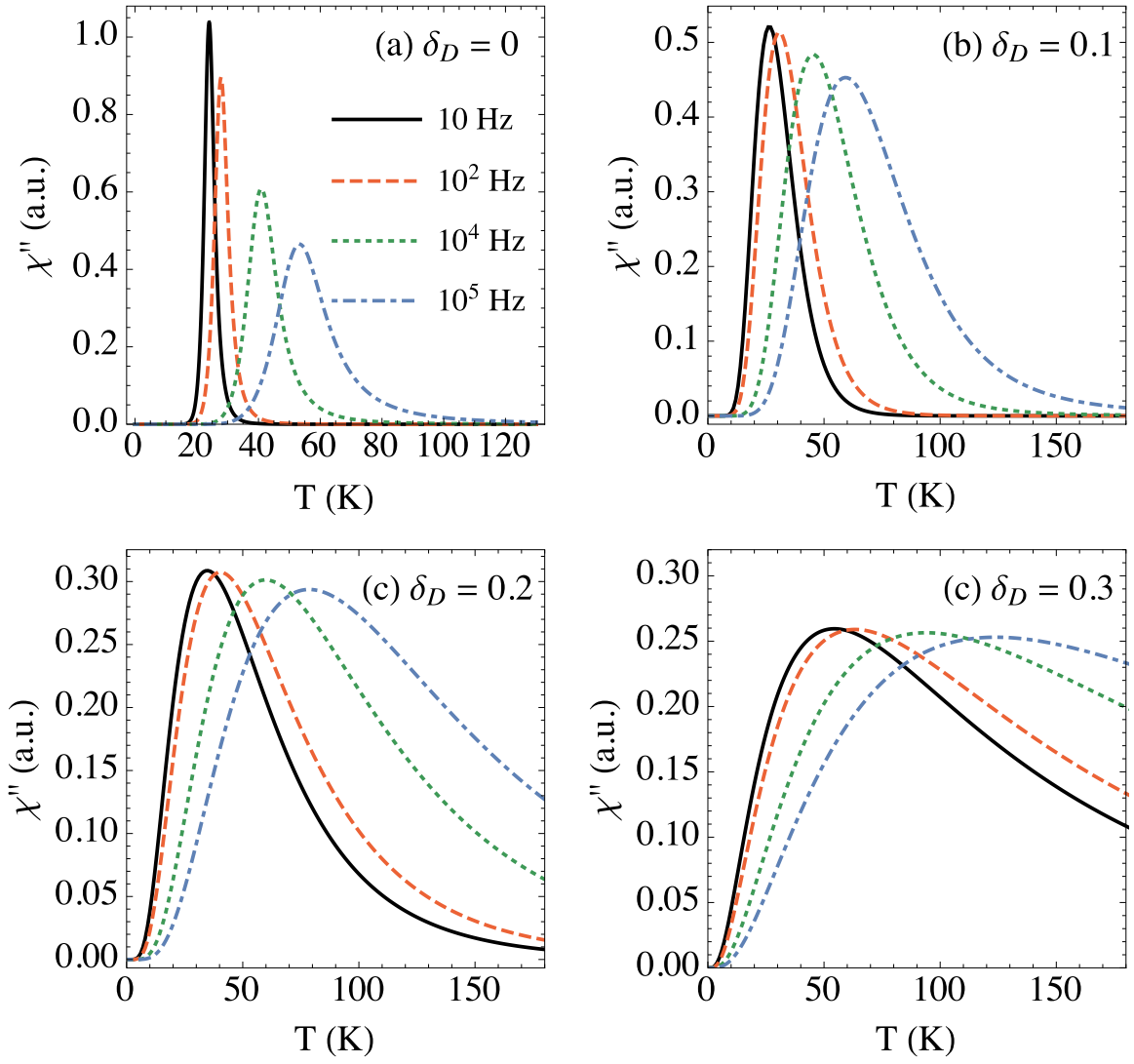

Fig. 1. Influence of the size distribution in $\chi''(T, f)$ curves for non-interacting samples. (a) Example curves of χ'' vs. T for ideal monodisperse samples computed from Eq. (3) with $\theta = 400$ K, $\tau_0 = 10^{-9}$ s and different values of f. (b)–(d) Same, but for polidisperse samples, computed from the numerical solution of the integral in Eq. (10), with $\theta_0 = 400$ K and three different values of δ_D.

Table 1
How the maximum of the imaginary part, $\chi''_{\max}$, behaves with the frequency f.

	Monodisperse	Polidisperse
Non-interacting	Decreases	Constant
Interacting	Inconclusive	Increases

distribution of volumes $P(V)$ will also be given by a lognormal distribution, which for spherical particles will have parameters $V_0 = \frac{\pi}{6} D_0^3$ and $\delta_V = 3\delta_D$ (for non-spherical particles only V_0 must to be modified). This property is unique of the lognormal distribution.

Assuming that the anisotropy constant K is the same for all particles, the energy barrier $\theta = KV/k_B$ will, for the same reason, also be given by a lognormal distribution

$$P(\theta) = \frac{1}{\sqrt{2\pi}\theta\delta_\theta} e^{-\frac{\ln^2(\theta/\theta_0)}{2\delta_\theta^2}} \tag{8}$$

with parameters

$$\theta_0 = \frac{KV_0}{k_B}, \quad \delta_\theta = \delta_V = 3\delta_D \tag{9}$$

The situation where K is not constant will be discussed in Section 2.5.

2.3. AC susceptibility for samples with a size distribution

We now average Eq. (3) over the size distribution $P(V)$, or what is equivalent, $P(\theta)$. In doing so, one must keep in mind that the signal picked up by a magnetometer is always proportional to the magnetic moment, never the magnetization. Hence, if one wishes to use $P(V)$ or $P(\theta)$, the average must be made over the magnetic moment. This determines the form of the static susceptibility χ_0 used in Eq. (4). For more information on this subtle point, see Ref. [59] and the supplemental information.

To perform the average it is more convenient to use $P(\theta)$. From the definitions $\theta = KV/k_B$ and $\theta_0 = KV_0/k_B$ we find that

$$\chi'' = N\frac{(M_s V_0)^2}{3k_B T}\int_0^\infty \frac{\theta^2}{\theta_0^2}\frac{\omega\tau(\theta/T)}{1+[\omega\tau(\theta/T)]^2}P(\theta)\,\mathrm{d}\theta \tag{10}$$

Numerical solutions of this integral are plotted in Figs. 1(b)–(d) for

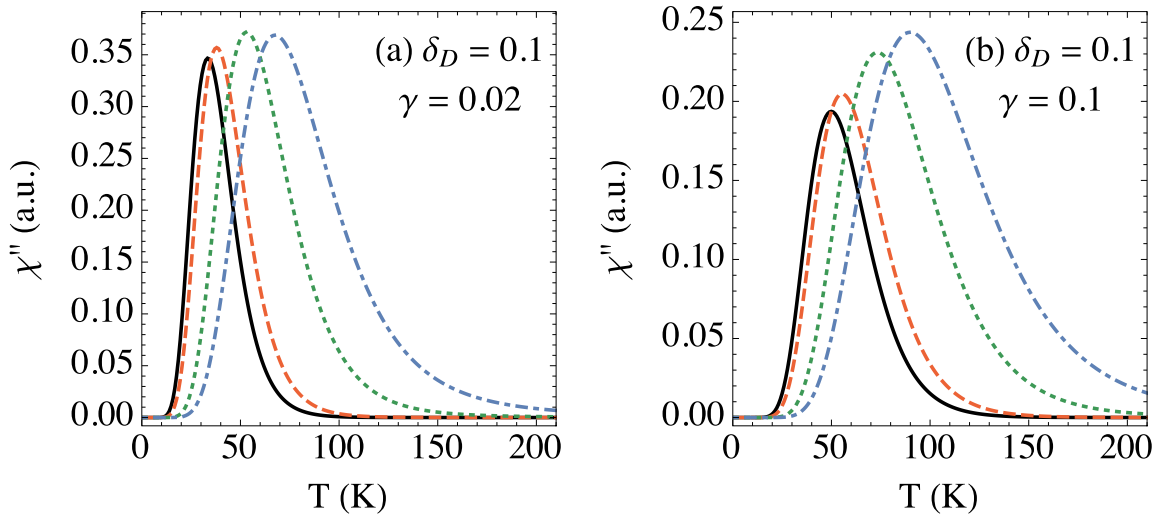

Fig. 2. Effect of the mean-field modification, Eq. (14), in the AC susceptibility curves. The simulation parameters are shown in the caption of each figure. The other parameters are the same as in Fig. 1.

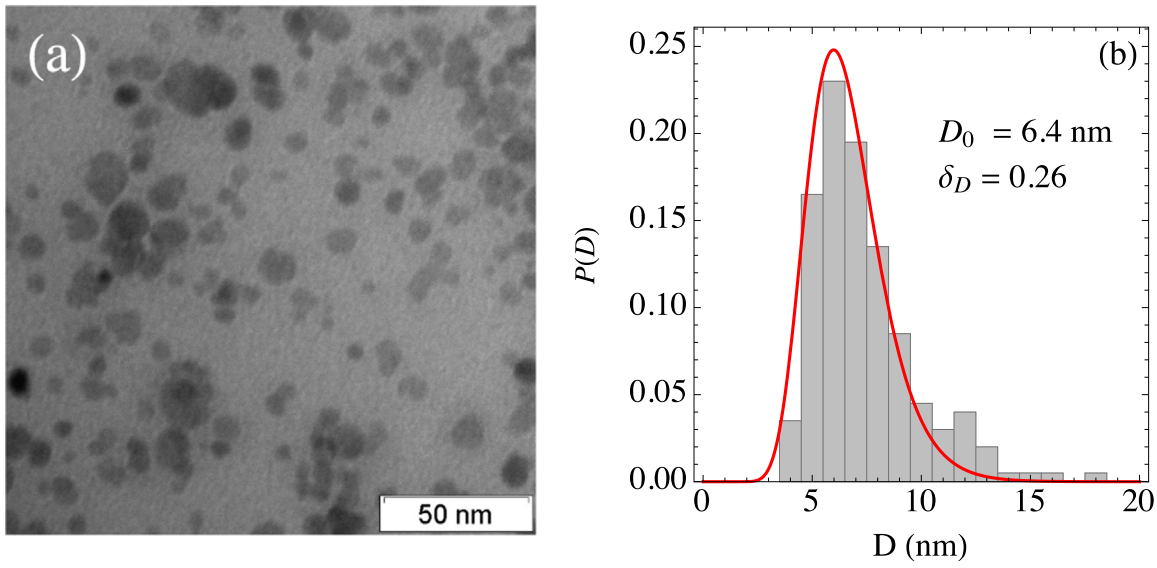

Fig. 3. (a) TEM micrograph of the commercial ferrofluid EMG909 from Ferrotec Co. (b) Corresponding size distribution and lognormal fit. Best fit parameters are shown in the figure.

several values of δ_D. In these figures it is possible to see the gradual effect which an increasing size dispersion has on the general shape of the curves.

Eq. (10) is exact, but cumbersome to work with. A more convenient approximate formula was obtained in Ref. [57] by noting that the function $\frac{\omega\tau}{1+(\omega\tau)^2}$ is sharply peaked around $\sigma^* = -\ln(2\pi f\tau_0)$. This leads to the following approximate expression for χ''

$$\chi'' = c\frac{\theta^*}{\theta_0^2}\exp\left\{-\frac{\ln^2(\theta^*/\theta_0)}{2\delta_\theta^2}\right\} \tag{11}$$

where $c = \sqrt{\frac{\pi}{2}}N(M_sV_0)^2/(6k_B\delta_\theta)$ is a positive constant and

$$\theta^* = \sigma^*T = -T\ln(2\pi f\tau_0) \tag{12}$$

The reason why θ_0^2 was not included in c is because it is the only term which depends on K and below, in Section 2.4, we will consider samples which have a distribution of K values.

Differentiating Eq. (11) with respect to $\theta^* = \sigma^*T$ we find that the maximum of χ'' occurs at $\theta_0 e^{\delta_\theta^2}$. This implies the relation

$$-\ln(2\pi f) = \ln(\tau_0) + \frac{\theta_0 e^{\delta_\theta^2}}{T_{\max}} \tag{13}$$

which shows that even for polidisperse samples an Arrhenius plot will still give a straight line. However, the slope of the line is given by $\theta_0 e^{\delta_\theta^2}$. For typical samples we have $\delta_D \sim 0.25$, which leads to $\delta_\theta = 3\delta_D \sim 0.75$ and thence $e^{\delta_\theta^2} \sim 1.75$. This shows that the Arrhenius plot overestimates the anisotropy constant K by a factor which can be almost of the order of 2 in certain cases.

We finish this section by noting that, in general, χ'' is a function of both f and T. However, under the approximations that led to Eq. (11), it turns out that χ'' will only depend on the particular combination $\theta^* = \sigma^*T = -T\ln(2\pi f\tau_0)$. This means that if we plot each χ'' curve as a function of θ^* instead of T, the data for different

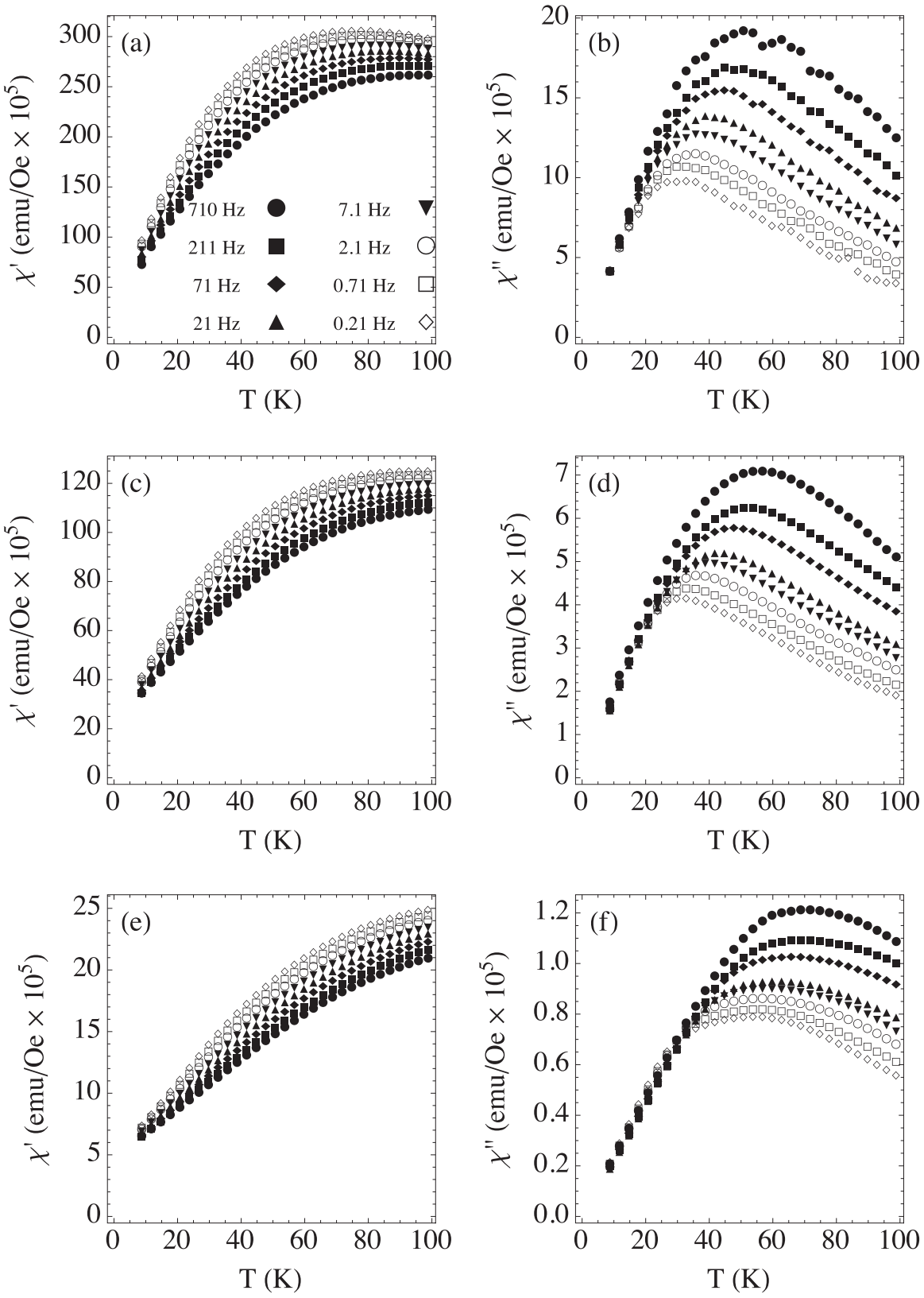

Fig. 4. Real (left) and imaginary (right) AC susceptibility data for several frequencies for the studied samples: (a,b) Sample A, 0.005%V/V, (c,d) Sample B, 0.540%V/V, and (e,f) Sample C, 3.600%V/V.

frequencies should all collapse into a single curve, provided τ_0 is correctly chosen. Hence, this method may be used to determine τ_0 and, since it uses the entire $\chi''(f, T)$ data set, it turns out to be much more precise than the Arrhenius plot. Examples of this are given below for our data in Figs. 4 and 9 or, e.g., in Refs. [33,57]. The collapsed data will be described by Eq. (11), which depends only on δ_θ, θ_0 and c. But $\delta_\theta = 3\delta_D$ is already known from TEM, so that the only two fit parameters are c and θ_0. Using Eq. (9)

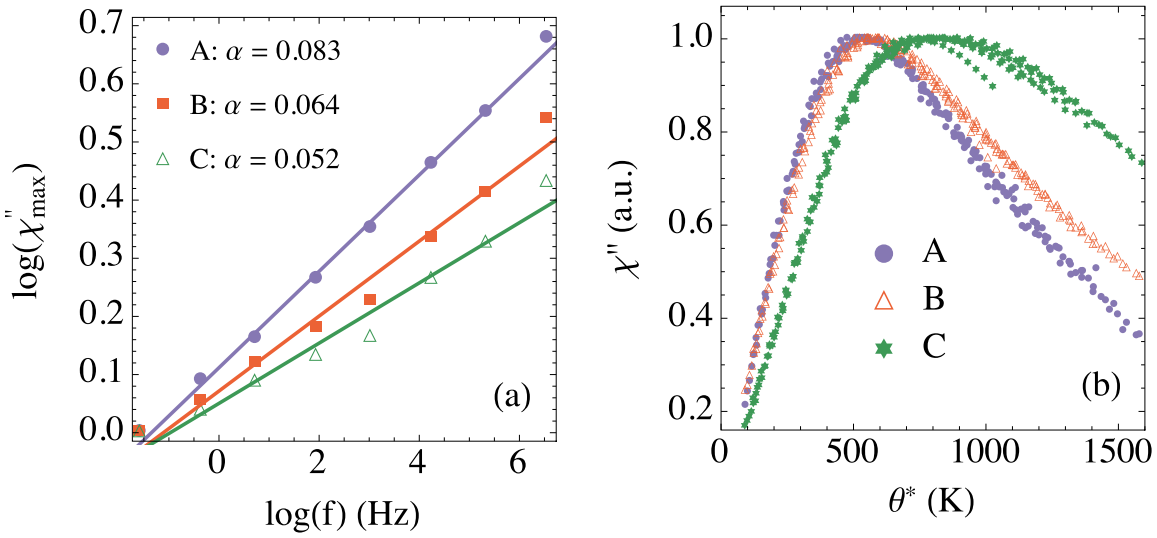

Fig. 5. (a) Log-log plot of the maximum of each χ'' curve as a function of the frequency f for the three samples. Each curve was normalized for visual purposes in order to start at the same point. The solid lines correspond to linear fits of Eq. (22) with exponents α shown in the figure. (b) Data collapse for samples A, B and C, obtained by plotting χ'' as a function of θ^*, defined in Eq. (18).

together with the value of V_0 obtained from TEM one may extract the anisotropy constant K.

2.4. Variation of $\chi''_{\max}$ with frequency

The usual Arrhenius analysis of AC susceptibility data focuses on the temperature $T_{\max}$ where χ'' is a maximum. We now argue that valuable information concerning the dipolar interaction is contained in the *height* $\chi''_{\max}$ of each χ'' vs. T maxima. In Fig. 1 we see two possible behaviors: For monodisperse samples, $\chi''_{\max}$ decreases with f, whereas for polidisperse samples, $\chi''_{\max}$ tends to become roughly constant, independent of f. These are the only two possibilities predicted by models of non-interacting single-domain particles.

However, in real samples it is also customary to find situations where $\chi''_{\max}$ *increases* with f. We argue that this is a signature of a strong dipolar interaction. It therefore serves as a simple test to estimate the relevance of this interaction in a given sample (this effect was briefly commented in Ref. [60]). If $\chi''_{\max}$ increases with f, the dipolar contribution certainly has a significant effect. For monodisperse samples this increase in $\chi''_{\max}$ competes with the natural tendency to decrease, so some care must be taken when interpreting the results (this competition was observed in numerical simulations in Ref. [61]). Table 1 summarizes the different possible behaviors. Please note that this rule is only valid for the imaginary part χ''. It does *not* hold for the real part χ'.

Our claim is corroborated by extensive experimental evidence in the literature. The most clear examples are Refs. [33,62–64,60], which study samples with different concentrations. In all cases the results are unambiguous: for diluted samples $\chi''_{\max}$ is either constant or diminishes with f, whereas for concentrated samples $\chi''_{\max}$ increases with f. Additional examples may also be found in Refs. [65–74] and in Figs. 4 and 9 below.

In order to better understand the frequency dependence of $\chi''_{\max}$ with f, we will now consider how Eq. (11) may be modified to include models of the dipolar interaction. A model which has been used extensively in the past is the Vogel-Fulcher law [25], whereby the energy barrier parameter σ is modified to account for the dipolar interaction according to $\sigma_{\rm VF} = \theta/(T - T_{\rm VF})$, where $T_{\rm VF}$ provides a measure of the strength of the dipolar interaction. The Vogel-Fulcher interaction gives good predictions when analyzed in terms of Arrhenius plots, but predicts zero susceptibility below $T_{\rm VF}$, something which is in clear disagreement with experiment.

Recently, one of the authors of this paper has worked out a mean-field model to describe the dipolar interaction which explicitly circumvents this difficulty [42]. The main result of this model is that, for sufficiently weak dipolar coupling, the anisotropy parameter should be modified according to

$$\sigma_{\rm MF} = \frac{\theta}{T} + \gamma\left(\frac{\theta}{T}\right)^2 \tag{14}$$

where

$$\gamma = \frac{N}{10}\left(\frac{\mu_0}{4\pi}\right)^2\left(\frac{\langle\mu^2\rangle}{KV_0}\right)^2\left\langle\frac{1}{R^6}\right\rangle \sim T_{\rm VF}/\theta_0 \tag{15}$$

is a dimensionless positive parameter representing the strength of the dipolar interaction. In this formula N is the number of particles in the sample, μ_0 is the vacuum permeability, $\langle\mu^2\rangle$ is the average magnetic moment squared in the sample and R is the random variable representing the distance between particles in the sample.

To study how this modification affects the AC curves we insert Eq. (14) in Eq. (10) and compute the integral numerically. The results are shown in Fig. 2 for parameters similar to those in Fig. 1. The tendency of the dipolar interaction to increase $\chi''_{\max}$ is clearly evident in this figure.

The mean-field approximation (14) is also more convenient than the Vogel-Fulcher model if one wishes to simplify the integral formula (10) as we did when deriving Eq. (11). If we retrace the same steps using instead $\sigma_{\rm MF}$ from Eq. (14), we find that

$$\chi'' = c\ \psi(f,\gamma)\frac{\theta^*}{\theta_0^2}\exp\left\{-\frac{\ln^2(\theta^*/\theta_0)}{2\delta_\theta^2}\right\} \tag{16}$$

where

$$\psi(f,\gamma) = \frac{1}{\sqrt{1 - 4\gamma\ln(2\pi f\tau_0)}} \tag{17}$$

and

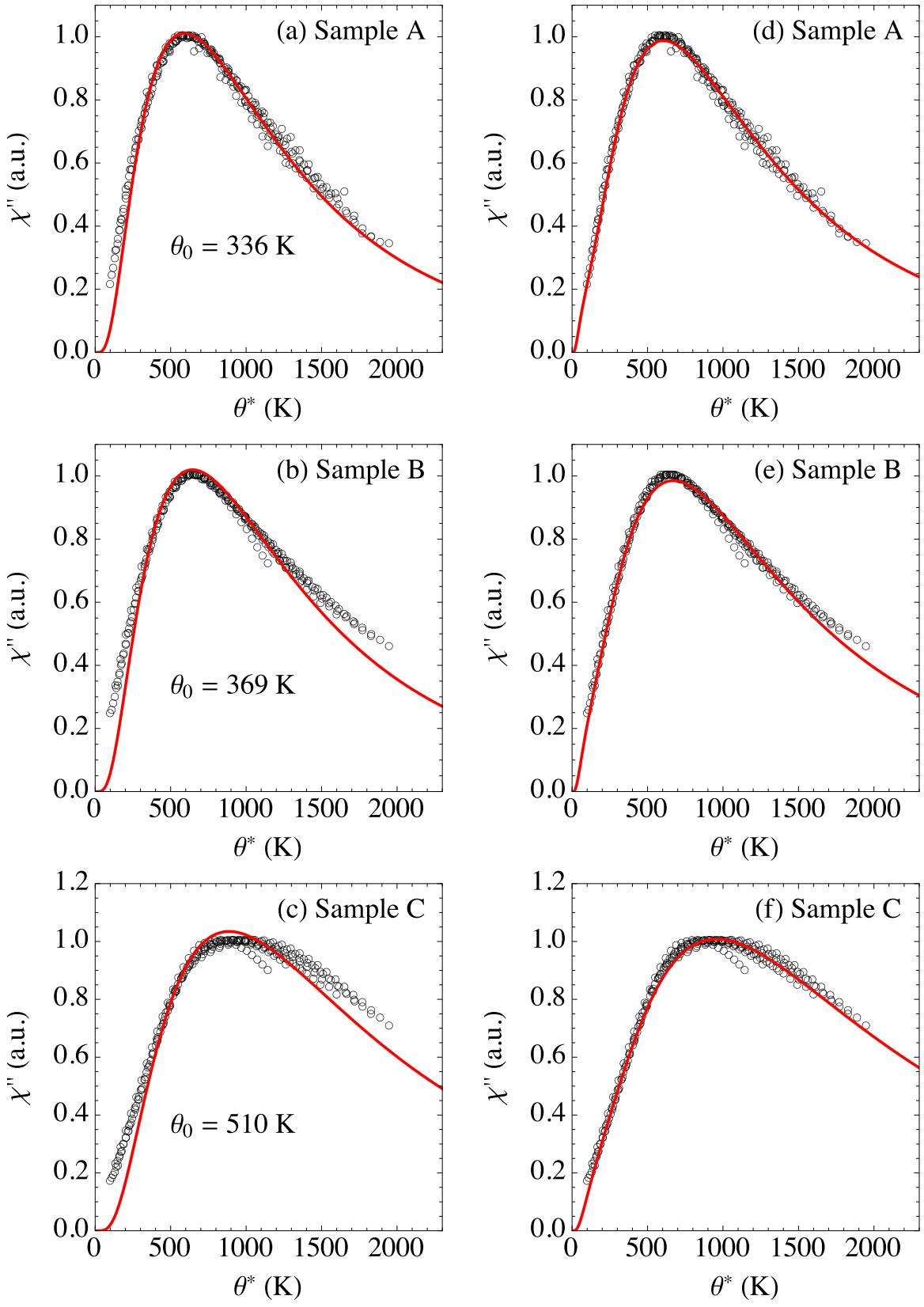

Fig. 6. Fit of Eq. (20) to the AC susceptibility data of samples A, B and C. Left panel: $n_K=1$. Right panel: $n_K=2$. Best fit results for the left panel are shown in each image and for the right panel in Table 2.

$$\theta^* = \frac{T}{2\gamma}\left[\sqrt{1 - 4\gamma \ln(2\pi f \tau_0)} - 1\right] \tag{18}$$

We therefore see that in the mean-field model an explicit dependence of $\chi''_{\max}$ on f appears through the function $\psi(f,\gamma)$. It predicts a roughly logarithmically increase with f.

Table 2
Best fit values of Eq. (20) for samples A, B and C when n_K=2.

Sample A		Sample B		Sample C	
$\theta_{0,i}$ (K)	q_i	$\theta_{0,i}$ (K)	q_i	$\theta_{0,i}$ (K)	q_i
67	0.026	89	0.039	137	0.04
387	0.974	438	0.961	625	0.96

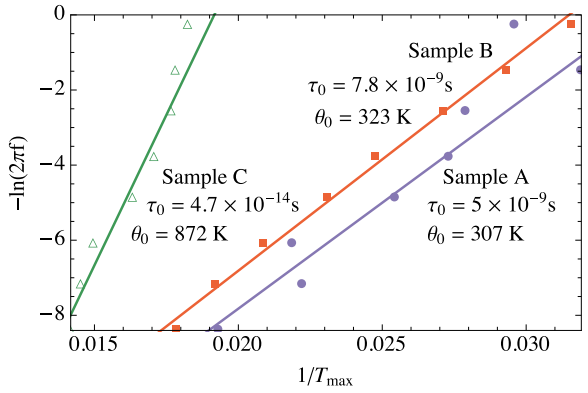

Fig. 7. Arrhenius plots [Eq. (13)] for samples A, B and C. The best fit parameters are shown in the figure.

Both previous models hold for weakly interacting systems. In the case of strong interactions, the Dorman-Bessais-Fiorani (DBF) model [29,75] predicts instead that the relaxation time of the system should be modified according to

$$\tau = \tau_0 e^{-n_1} \exp\left\{\sigma\left(1 + \frac{n_1 a_1 M_s^2}{K}\right)\right\} \tag{19}$$

where n_1 is the number of nearest neighbors and a_1 is the volume concentration of particles in the sample. This model therefore predicts that τ_0 should be effectively reduced by a factor e^{-n_1}. This is in accordance with the unphysically low τ_0 values which are sometimes obtained using Arrhenius plots.

Lastly, it must be mentioned that more recent theoretical models [76,77] have also been considered. Unfortunately, despite their success in explaining other physical properties, they were found not to provide additional contribution to our particular analysis of the AC susceptibility.

2.5. Distribution of anisotropy constants

As discussed in Section 1, in addition to the usual contribution from the dipolar interaction, we must also consider the distribution of anisotropy constants caused by the formation of aggregates. The particles in a sample are either in free suspension in the fluid or reside in clusters of different sizes [53]. Depending on the size of the cluster and the position of the particle within that cluster, it may experience a different modification to its anisotropy constant K [10,54]. We therefore see that, in addition to the distribution of volumes in a given sample, we should also expect to have a very complex distribution of K values.

To include this effect, we must perform a second average of Eq. (16) over a distribution of K. This distribution is certainly continuous, but we have no information about it to be able to propose an analytical formula. Hence, we will for simplicity assume that the distribution of anisotropy constants is discrete. That is, we will assume that in the sample there is a fraction q_1 of particles which have an anisotropy constant K_1, a fraction q_2 with constant K_2, etc. This rough approximation should serve as a seed for future work, when the distribution of anisotropies in interacting systems is better understood.

In order to obtain a tractable equation, we will also assume that γ defined in Eq. (15) is the same for all K, an approximation which is justified due to the smallness of γ. We then obtain, instead of Eq. (16),

$$\chi'' = c\ \psi(f,\gamma) \sum_{i=1}^{n_K} q_i \frac{\theta^*}{\theta_{0,i}^2} \exp\left\{-\frac{\ln^2(\theta^*/\theta_{0,i})}{2\delta_\theta^2}\right\} \tag{20}$$

where n_K is the total number of distinct K values we wish to consider and

$$\theta_{0,i} = \frac{K_i V_0}{k_B} \tag{21}$$

with V_0 being known from TEM. Eq. (20) can be fitted to the collapsed data, with parameters c, q_i and $\theta_{0,i}$ (the value of δ_θ is fixed from TEM).

3. Experiments

We now apply Eq. (20) to two distinct samples. In Section 3.1 we study a commercial ferrofluid containing spherical magnetite nanoparticles of roughly 6.4 nm in diameter and in Section 3.2 we study a sample of cubic magnetite nanoparticles with about 13 nm loaded on the surface of polymeric nanospheres. Both samples are studied under different dilutions.

3.1. Magnetite nanoparticles in a ferrofluid

We begin with the commercial ferrofluid EMG909 from Ferrotec Co, consisting of roughly spherical magnetite particles dispersed in oil (isoparaffin). A typical TEM micrograph is shown in Fig. 3 together with the size distribution histogram and lognormal fit. The best fit parameters were $D_0 = 6.4$ nm and $\delta_D = 0.26$. Thus, the mean diameter is 6.6 nm and the dispersion of the energy barrier distribution is $\delta_\theta = 3\delta_D = 0.78$.

We have performed AC susceptibility measurements for three dilutions, named samples A, B and C, with volume concentrations of 0.005%, 0.540% and 3.600%. The measurements were performed in an MPMS-7T system from Quantum Design under a field amplitude of 2.0 Oe (0.16 kA/m). The samples were placed into quartz tubes sealed with a dental composite resin, and no correction due do the diamagnetic contribution of the oil and the sample holder was necessary, since the ferromagnetic signal of MNPs dominated even for the more diluted sample. The raw data for the real and imaginary susceptibilities are shown in Fig. 4 for the three samples. As can be seen, the maximum height χ''_{max} increases substantially with f, indicating the presence of the dipolar interaction, even in the most diluted sample.

In Fig. 5(a) we present a log-log plot of the maximum height, χ''_{max}, of each χ'' vs. T curve as a function of the frequency f. The approximate linearity of the data in a log-log plot suggests that χ''_{max} scales with f following a power law

$$\chi''_{max} \sim f^{\alpha} \tag{22}$$

for some exponent α. The values of α obtained from a linear fit were 0.083, 0.064 and 0.052 for samples A, B and C respectively. This behavior is quite different from that predicted by the mean-field model [Eq. (17)], whereby χ''_{max} should depend only logarithmically on f. This discrepancy is attributed to the fact that the mean-field model should hold only for weakly-interacting particles. In Fig. 5 we also see some deviations from the power law behavior, specially for samples B and C. This shows that such a

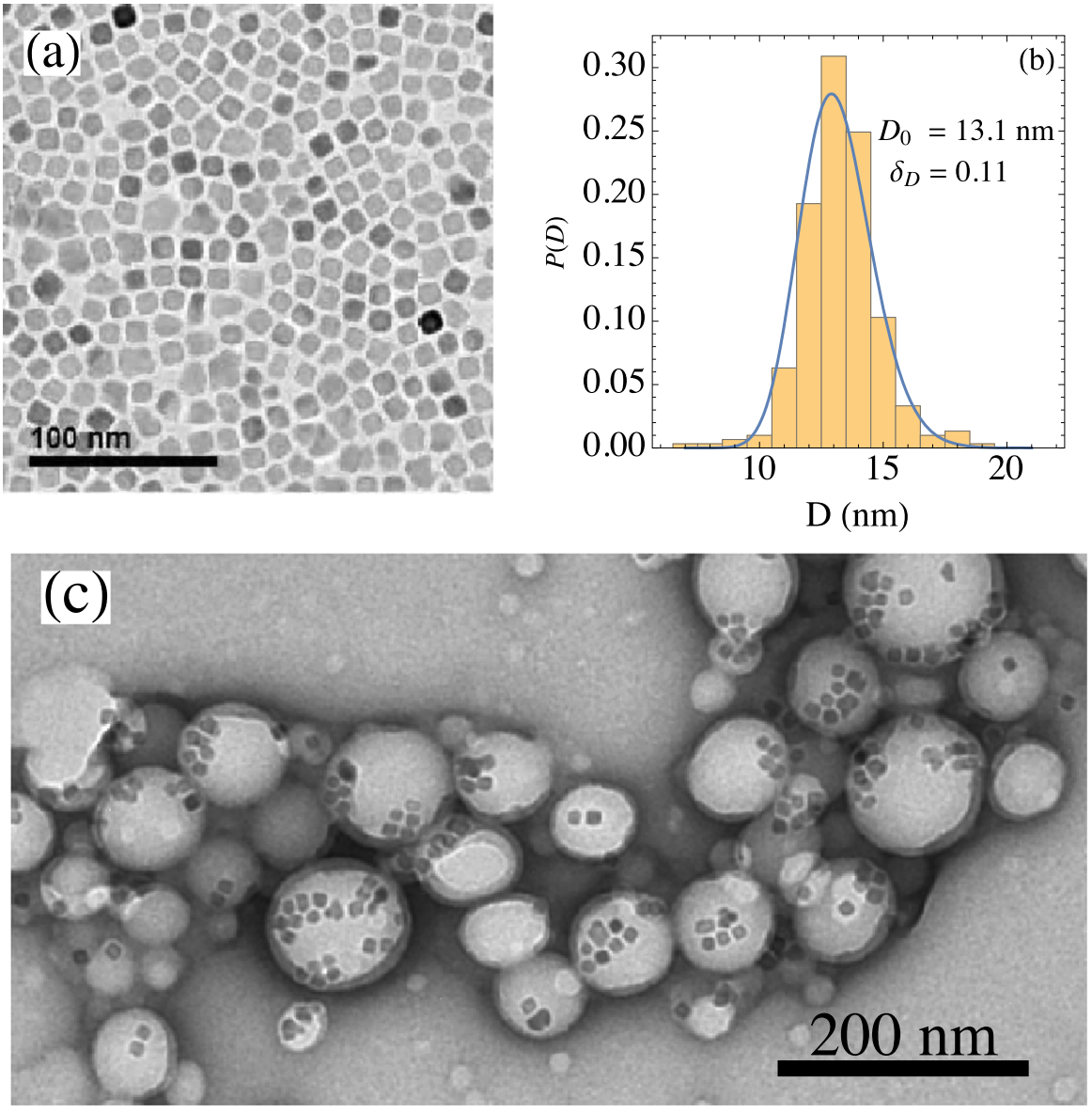

Fig. 8. (a) TEM micrograph of cubic magnetite nanoparticles. (b) Distribution of face diagonals D and corresponding lognormal fit. The best fit parameters are shown in the figure. (c) TEM micrograph showing an example of the nanoparticles loaded on the PLGA nanospheres. The nanospheres were negatively stained to improve contrast [12].

scaling form should be considered only as a rough first approximation to a much more complex behavior.

Next, we perform a data collapse of the χ'' data. To do so, we first normalize all curves to have the same height since this aspect has already been analyzed in Eq. (22). Using the expression of θ^* for interacting samples, given in Eq. (18), the collapse yields $\tau_0 = 2 \times 10^{-9}$ s and $\gamma = 0.01$, 0.01 and 0.0115 for samples A, B and C respectively. The collapsed data is shown in Fig. 5(b). If we use instead the non-interacting formula in Eq. (12), we obtain $\tau_0 = 2 \times 10^{-10}$ s. Hence, we see that by neglecting the dipolar interaction we underestimate τ_0 by one order of magnitude. According to Eq. (19) the presence of the dipolar interaction should modify τ_0 by a factor e^{-n_1}, where n_1 is the average number of nearest neighbors. Thus, we may estimate this value by analyzing the ratio between our two estimates of τ_0, the one with the dipolar interaction and the one without it. As a result we get $n_1 \simeq 2.3$.

From the collapsed data set we may proceed to use Eq. (20) and study the aggregation of particles within the sample. From TEM we already know that $\delta_\theta = 3\delta_D = 0.78$ so the only free parameters are $\theta_{0,i}$, q_i and c. The results for $n_K=1$ are shown in the left panel of Fig. 6 and the best fit values of θ_0 are presented in each image. A clear disagreement between the fitted curve and the experimental data can be observed. The situation is particularly worse at low temperatures, where the signal from smaller particles is expected to be stronger.

Next we attempt to fit Eq. (20) using $n_K=2$. The results are shown in the right panel of Fig. 6 and the best fit parameters are presented in Table 2. As can be seen, in this case the agreement with the experimental data is remarkably good. From Table 2 we see that both $\theta_{0,1}$ and $\theta_{0,2}$ increase with concentration, indicating that the dipolar interaction shifts the energy barrier distribution of the particles to higher values. In Table 2 we also report the fractions q_i, showing that the majority of the particles have a high anisotropy. Notwithstanding, since Eq. (20) depends on $1/\theta_{0,i}^2$, the small fraction q_1 still gives a significant contribution to the AC susceptibility curve, specially at low temperatures.

From the values reported in Table 2 for $\theta_{0,1}$ and $\theta_{0,2}$ we may then compute the anisotropy constants from the relations $\theta_{0,i} = K_i V_0/k_B$. For this sample $k_B/V_0 \simeq 1000$ erg/(K cm^3) = 0.1 kJ/(K m^3). Hence, we

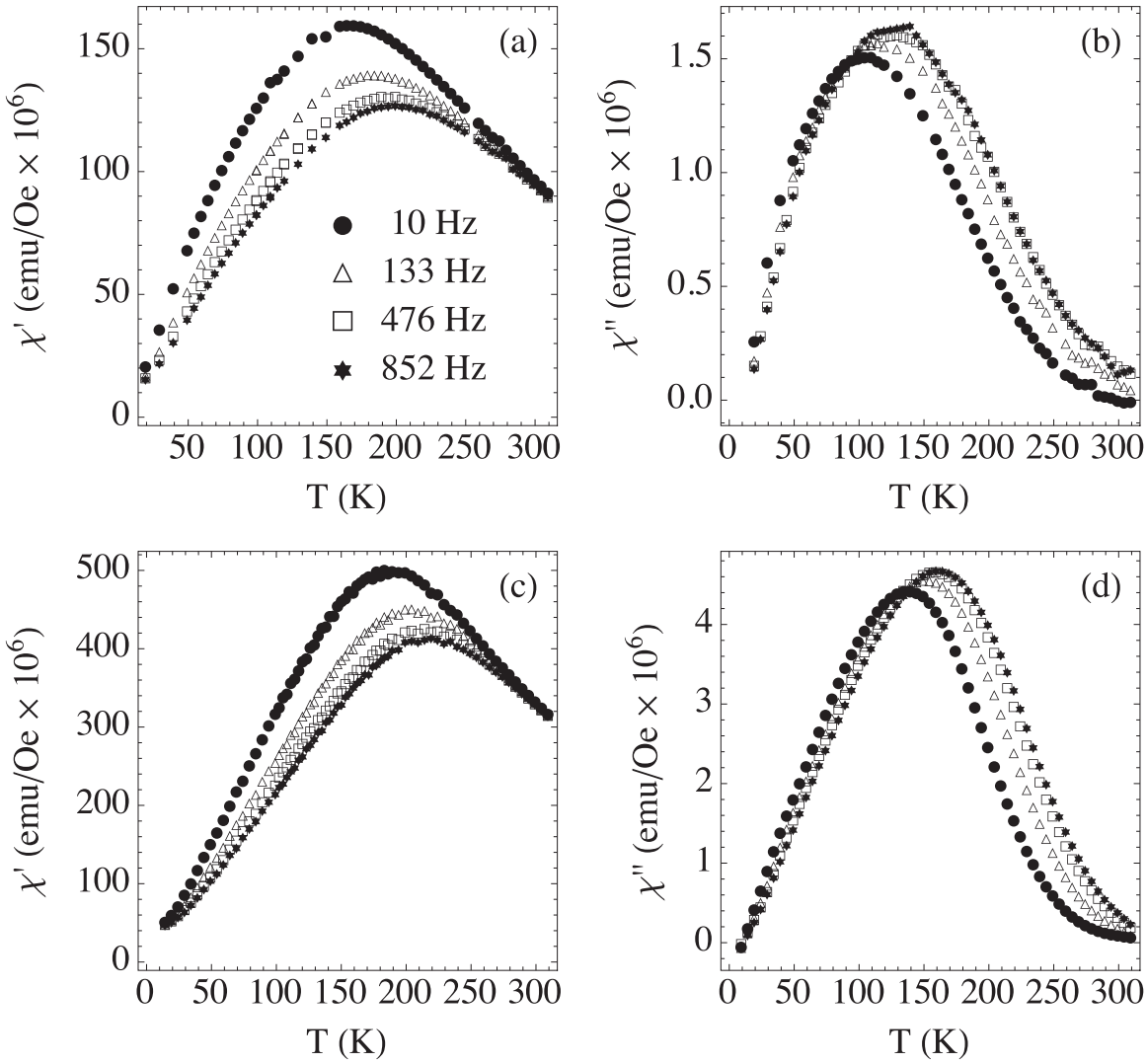

Fig. 9. Real (left) and imaginary (right) AC susceptibility data for the polymeric nanopsheres: (a,b) sample L, dispersed in water, 0.001%V/V, and (c,d) sample S, lyophilized, concentration 0.783%V/V.

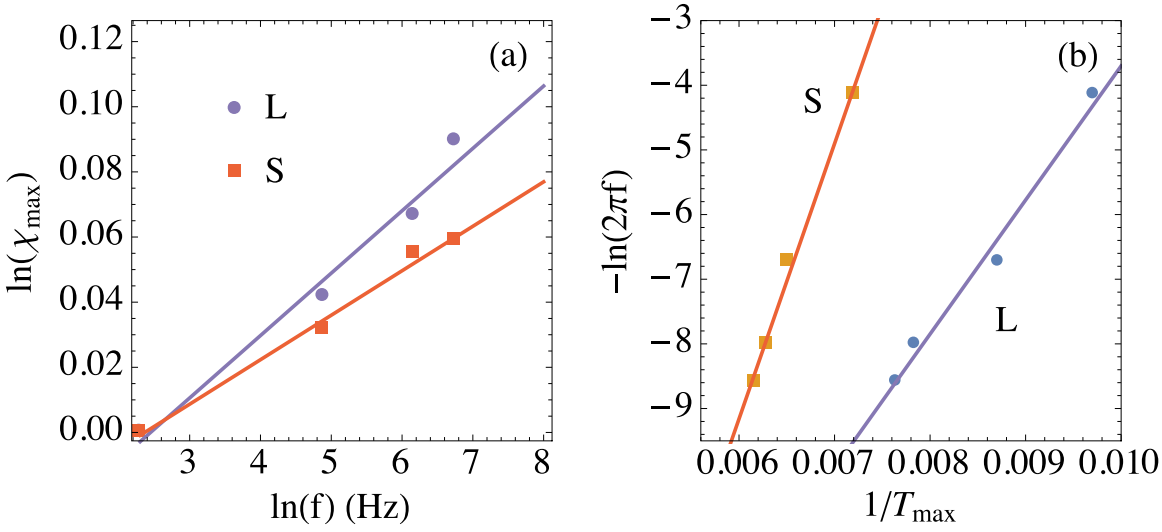

Fig. 10. (a) Maximum height χ''_{max} as a function of f (normalized by the first frequency point). (b) Arrhenius plot with best fit parameters $\tau_0 = 2.5 \times 10^{-11}$ s and $\theta_0 = 2070$ K for sample L and $\tau_0 = 8.6 \times 10^{-16}$ s and $\theta_0 = 4260$ K for sample S.

conclude that the particles reside in two main types of aggregates: ones with anisotropy constants between 6 and 14 kJ/m^3 and others with anisotropy constants between 38 and 63 kJ/m^3.

We therefore observe a roughly 5-fold increase in the effective anisotropy constants between the two populations. It is also observed that the K_i for a given population increases with concentration (A to C). If we assume that an increase in concentration implies the formation of larger clusters, then this result would suggest that larger clusters display higher K_i values. Also, if we assume that larger particles may have a tendency to form larger clusters, it is not illogical to assign the higher K_i values to the biggest particles. However, this result must be taken with care, since it is not illogical either to assign the higher K_i values to the smallest particles, whose surface anisotropy can be high and dominant.

For completeness, we present in Fig. 7 an Arrhenius plot [cf. Eq. (13)] for the three samples. The corresponding best-fit parameters are shown in the figure. As can be seen, the Arrhenius plot fits the experimental data with a straight line, although it also predicts different values of τ_0 for each dilution, which does not have a physical meaning. Moreover, the values of θ_0 are somewhat similar to those obtained using $n_K=1$ in the left part of Fig. 6.

3.2. Magnetite nanoparticles embedded in nanospheres

Next we consider the case of PLGA [the poly(D,L-lactide-*co*-glycolic) acid copolymer] nanospheres, loaded with cubic magnetite nanoparticles on their surface. Magnetite nanocubes were first obtained by thermal decomposition of iron-based organic precursors, with a seeded growth method modified from the original one of Sun et al. [78] and using oleic acid and oleylamine as surfactants. Afterwards, a solution containing the nanocubes and PLGA was used as the organic phase in a procedure combining miniemulsion and solvent evaporation [79] to obtain PLGA nanospheres loaded with nanocubes. More details of the synthesis and additional characterizations can be found in Ref. [12].

Fig. 8 shows a typical TEM image of the particles together with the size distribution histogram and the lognormal fit. The best fit parameters were $D_0 = 13.1$ nm and $\delta_D = 0.11$, showing that the size distribution is very narrow. Indeed, referring to Eq. (7), we see that these nano-cubes may be considered as monodisperse [12]. It is worth mentioning that all results developed in Section 2 also hold for cubic particles, provided we now use $V_0 = D_0^3/2^{3/2}$ where D_0 is the face diagonal of the cubes.

In Fig. 8(c) we also show an example of the PLGA nanospheres loaded with MNPs. This TEM image was obtained using a negative staining procedure (as described in Ref. [12]) for better visibility of the nanospheres, and shows how the confinement of the nanoparticles on the polymeric nanospheres allows maintaining 2-dimensional aggregates on their surface. This superficial distribution can be easily inferred from TEM images, since nanocubes appear with high contrast, non-overlapped and it is even possible to observe nanocubes protruding from the nanospheres.

We prepared two samples with the same polymeric nanospheres, one where they were dispersed in water and the other with them lyophilized to form a powder. We shall refer to them as samples L and S respectively. In these samples, the nanocube arrangements are preserved, but the inter-sphere distance is changed (shorter in S). The volume concentration of magnetic material is 0.001% and 0.783% respectively for samples L and S.

AC susceptibility data was acquired with an MPMS-XL SQUID magnetometer from Quantum design under a field amplitude of 2.74 Oe (0.22 kA/m). In Fig. 9 we present the raw susceptibility data for both samples and several frequencies. As can be seen, for both samples there is a sensitive dependence of $\chi''_{\max}$ with the height, indicating the presence of a sizable dipolar contribution.

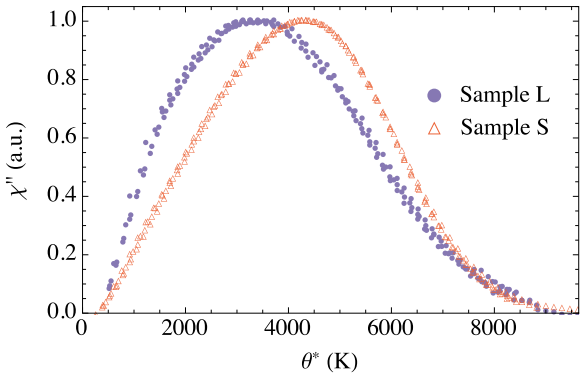

Fig. 11. Data collapse for samples L and S, obtained by plotting χ'' as a function of θ^*, defined in Eq. (18). From the collapse we find $\tau_0 = 4 \times 10^{-10}$ s and $\gamma = 0.6$ and 0.9 for samples L and S respectively.

We begin, as before, by analyzing the dependence of $\chi''_{\max}$ with f. The results are shown in Fig. 10(a) where we again observe an approximate power law behavior [cf. Eq. (22)], with exponents $\alpha = 0.019$ and 0.013 for samples L and S respectively.

We also perform an Arrhenius plot shown in Fig. 10(b). The linear fit yields $\tau_0 = 2.5 \times 10^{-11}$ s and $\theta_0 \simeq 2000$ K for sample L and $\tau_0 = 8.6 \times 10^{-16}$ s and $\theta_0 \simeq 4200$ K for sample S. We therefore see a clear discrepancy in the τ_0 values, which should be the same since both samples are composed by the exact same particles. Moreover, we see that for sample S the value of τ_0 is clearly unphysical. This is again a manifestation of the influence of the dipolar interaction in estimating τ_0.

This problem with τ_0 can be resolved by performing the data collapse using Eq. (18). In this case we find $\tau_0 = 4 \times 10^{-10}$ s and $\gamma = 0.6$ and 0.9 for samples L and S respectively. The collapse curve is shown in Fig. 11. If we use instead Eq. (12) to perform the collapse, we find $\tau_0 = 5 \times 10^{-16}$ s, which is similar to that obtained in the Arrhenius analysis. The number of nearest neighbors may again be estimated by comparing the τ_0 values obtained by the two different models and using Eq. (19). As a result, we find $n_1 \simeq 13.8$. Despite being overestimated, this result indicates that the DBF model correlates qualitatively with the groups of nanocubes found in the nanospheres [cf. Fig. 8(c)].

We now fit Eq. (20) to the collapsed data in Fig. 11 using $\delta_\theta = 3\delta_D = 0.33$, as obtained from TEM. The fits were performed using $n_K=1$, 2 and 3 and the results are shown in Fig. 12, for sample L in the left panel and sample S in the right panel. The corresponding best fit parameters are summarized in Table 3. As can be seen, there is a strong disagreement between the best fitted function and the experimental data when $n_K=1$ [images (a) and (d)]. The same is true for $n_K=2$, despite a visible improvement. It is only for $n_K=3$ that the fitted curve begins to resemble the real data. For $n_K=3$ the results are better for sample L than sample S, in agreement with our intuition that for sample S the distribution of K values should be much more complex due to the increase of inter-sphere interactions. Increasing n_K above 3 does not improve the results in any way. The values of K may be computed using $\theta_{0,i}$ from Table 3 are roughly 15, 32 and 64 kJ/m^3.

Concerning the results for $n_K=3$, shown in Table 3, we see that when going from sample L to sample S the energy barriers remain roughly unaltered and only the population of each cluster change. This is in agreement with the fact that both samples have the same nanoparticle arrangement.

The existence of at least three populations in these samples can be assigned to the different arrangements acquired by the particles on the nanospheres surface, either in single chains, or in 2D arrangements involving a diverse number of particles [cf. Fig. 8(c)].

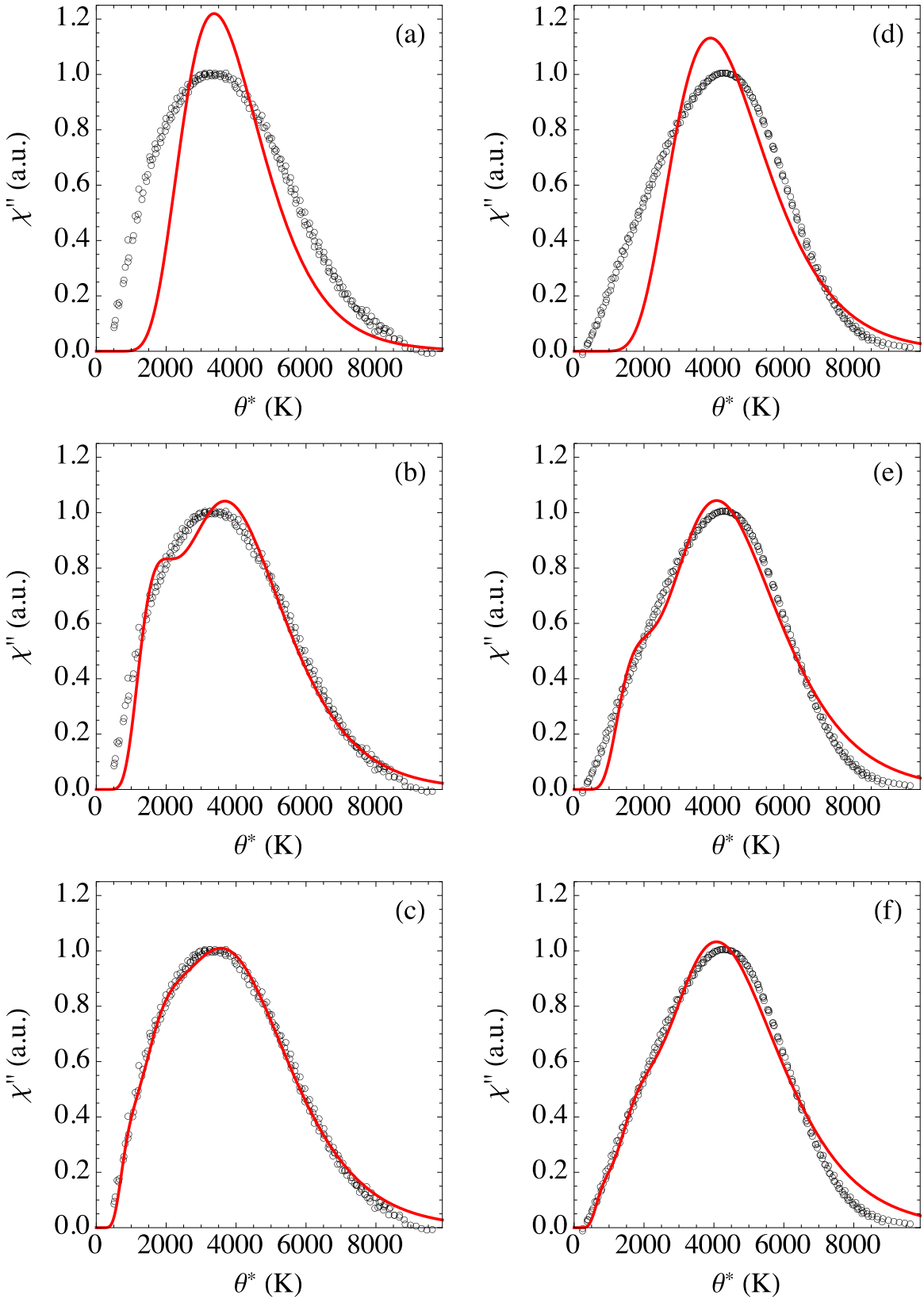

Fig. 12. Fit of Eq. (20) to the susceptibility data of samples L (left panel) and S (right panel). (a) and (d) $n_K=1$; (b) and (e) $n_K=2$; (c) and (f) $n_K=3$. The best fit parameters are summarized in Table 3.

Table 3
Best fit values of Eq. (20) for samples L and S, with different values of n_K.

n_K	Sample L		Sample S	
	$\theta_{0,i}$ (K)	q_i	$\theta_{0,i}$ (K)	q_i
1	3000	1	3470	1
2	1540	0.25	1610	0.17
	3440	0.75	3710	0.83
3	920	0.064	820	0.0258
	1830	0.261	1760	0.166
	3590	0.675	3750	0.8082

Such arrangements can present different magnetic configurations [80], giving rise to different K_i values.

4. Discussion and conclusions

The purpose of this paper was to show how AC susceptibility may be used to extract information concerning the presence of the dipolar interaction in a sample. As we have argued, in samples where the particles are left in fluid suspension or packed inside nano-carriers, the dipolar interaction manifests itself in two separate ways. The first is the direct dipolar effect, which can be modeled, for instance, using the Vogel-Fulcher, mean-field or DBF models, as discussed in Section 2.4. In addition, the dipolar interaction also manifests itself by inducing the formation of clusters of particles within the sample. Once in a cluster, the effective anisotropy of a particle will be strongly modified due to its proximity with the other particles.

Practically all models and papers discussing the dipolar interaction focus only on the first aspect. Our intention was to emphasize the role of the second aspect as well, specially for samples which are of importance for biological applications. We have introduced the idea that this effect can be modeled by including, in addition to the volume distribution usually obtained from TEM, a distribution of anisotropy constants. It was also the purpose of this paper to draw attention to the dependence of $\chi''_{\max}$ with f. This, as we have shown, provides a very simple visual tool to estimate the relevance of the dipolar interaction when analyzing a given sample.

To summarize the procedure adopted here, from a visual analysis $\chi''_{\max}$ vs. f one estimates the importance of the dipolar interaction in that sample. Then, using a data collapse with Eq. (18) one can estimate τ_0 and obtain the mean-field interaction constants γ defined in Eq. (15) and the mean number of nearest-neighbors n_1 using Eq. (19). Finally, by fitting the collapsed data using Eq. (20) one is able to probe the complexity of the dipolar landscape and estimate the anisotropy constant distribution in the sample.

Acknowledgements

For their financial support, the authors would like to acknowledge the Brazilian funding agencies FAPESP, CNPq and FAPEG, the funding agencies Spanish MINECO and FEDER, under project MAT2014-53961-R. I. Andreu thanks the Spanish CSIC for her JAE Predoc contract. Finally, we thank Prof. S. M. Carneiro for her help with the TEM images of the spherical magnetite nanoparticles.

Appendix A. Supplementary data

Supplementary data associated with this article can be found in the online version at http://dx.doi.org/10.1016/j.jmmm.2016.08.011.

References

[1] K.M. Krishnan, IEEE Trans. Magn. 46 (2010) 2523.
[2] J. Dobson, Nano Today 2 (2006) 22.
[3] C.-W. Lu, Y. Hung, J.-K. Hsiao, M. Yao, T.-H. Chung, Y.-S. Lin, S.-H. Wu, S.-C. Hsu, H.-M. Liu, C.-Y. Mou, C.-S. Yang, D.-M. Huang, Y.-C. Chen, Nano Lett. 7 (2007) 149.
[4] J.W. Bulte, T. Douglas, B. Witwer, S.C. Zhang, E. Strable, B.K. Lewis, H. Zywicke, B. Miller, P. van G, B.M. Moskowitz, I.D. Duncan, J.A. Frank, Nat. Biotechnol. 19 (2001) 1141.
[5] B.A. Larsen, M.A. Haag, N.J. Serkova, K.R. Shroyer, C.R. Stoldt, Nanotechnology 19 (2008) 265102.
[6] R.K. Gilchrist, R. Medal, W.D. Shorey, R.C. Hanselman, J.C. Parrott, C.B. Taylor, Ann. Surg. 146 (1957) 596.
[7] I. Hilger, R. Hergt, Nanobiotechnol. IEE 152 (2005) 33.
[8] Q.A. Pankhurst, N.K.T. Thanh, S.K. Jones, J. Dobson, J. Phys. D: Appl. Phys. 42 (2009) 224001.
[9] J.-H. Lee, J.-T. Jang, J.-S. Choi, S.H. Moon, S.-H. Noh, J.-W. Kim, J.-G. Kim, I.-S. Kim, K.I. Park, J. Cheon, Nat. Nanotechnol. 6 (2011) 418.
[10] L.C. Branquinho, M.S. Carrião, A.S. Costa, N. Zufelato, M.H. Sousa, R. Miotto, R. Ivkov, A.F. Bakuzis, Sci. Rep. 3 (2013) 2887.
[11] I. Andreu, E. Natividad, L. Solozábal, O. Roubeau, J. Magn. Magn. Mater. 380 (2015) 341.
[12] I. Andreu, E. Natividad, L. Solozábal, O. Roubeau, ACS Nano 9 (2015) 1408.
[13] H.F. Rodrigues, F.M. Mello, L.C. Branquinho, N. Zufelato, E.P. Silveira-Lacerda, A. F. Bakuzis, Int. J. Hyperth. 29 (2013) 752.
[14] C.L. Dennis, A.J. Jackson, J.A. Borchers, P.J. Hoopes, R. Strawbridge, A. R. Foreman, J. van Lierop, C. Grüttner, R. Ivkov, Nanotechnology 20 (2009) 395103.
[15] K. Maier-Hauff, F. Ulrich, D. Nestler, H. Niehoff, P. Wust, B. Thiesen, H. Orawa, V. Budach, A. Jordan, J. Neuro-Oncol. 103 (2011) 317.
[16] (a) W.F. Brown, Phys. Rev. 130 (1963) 1677;
(b) W.F. Brown, IEEE Trans. Magn. 15 (1979) 1196.
[17] W.T. Coffey, Y.P. Kalmykov, J.T. Waldron, The Langevin Equation. With Applications to Stochastic Problems in Physics Chemistry and Electrical Engineering, 2nd ed., World Scientific Publishing Co. Pte. Ltd., Singapore 2004, p. 678.
[18] W.T. Coffey, D.S.F. Crothers, Y.P. Kalmykov, J. Magn. 127 (1993) 254;
W.T. Coffey, Y.P. Kalmykov, J. Appl. Phys. (2012), http://dx.doi.org/10.1063/1.4754272.
[19] J.L. Garcıa-Palacios, F.J. Lázaro, Phys. Rev. B 58 (1998) 14937;
J.L. Garcia-Palacios, P. Svedlindh, Phys. Rev. Lett. 85 (2000) 3724.
[20] Y.P. Kalmykov, S.V. Titov, Phys. Solid State 41 (1999) 1854;
Y.P. Kalmykov, W.T. Coffey, U. Atxitia, O. Chubykalo-Fesenko, P.-M. Déjardin, R. W. Chantrell, Phys. Rev. B 82 (2010) 024412.
[21] I.S. Poperechny, Y.L. Raikher, V.I. Stepanov, Phys. Rev. B 82 (2010) 174423.
[22] G.T. Landi, J. Magn. Magn. Mater. 324 (2012) 466;
G.T. Landi, A.D. Santos, J. Appl. Phys. 111 (2012) 07D121;
G.T. Landi, J. Appl. Phys. 111 (2012) 043901.
[23] J. Carrey, B. Mehdaoui, M. Respaud, J. Appl. Phys. 109 (2011) 083921.
[24] E.L. Verde, G.T. Landi, J.A. Gomes, M.H. Sousa, A.F. Bakuzis, J. Appl. Phys. 111 (2012) 123902;
E.L. Verde, G.T. Landi, M.S. Carrião, A.L. Drummond, J.A. Gomes, E.D. Vieira, M. H. Sousa, A.F. Bakuzis, AIP Adv. 2 (2012) 032120;
G.T. Landi, A.F. Bakuzis, J. Appl. Phys. 111 (2012) 083915.
[25] S. Shtrikman, E.P. Wohlfarth, Phys. Lett. A 85 (1981) 467.
[26] R.W. Chantrell, E.P. Wohlfarth, J. Magn. Magn. Mater. 40 (1983) 1.
[27] T. Jonsson, J. Mattsson, C. Djurberg, F.A. Khan, P. Nordblad, P. Svedlindh, Phys. Rev. Lett. 75 (1995) 4138.
[28] P. Jönsson, J. García-Palacios, Phys. Rev. B 64 (2001) 174416.
[29] J.L. Dormann, F. D'Orazio, F. Lucari, E. Tronc, P. Prené, J.P. Jolivet, D. Fiorani, R. Cherkaoui, M. Noguès, Phys. Rev. B 53 (1996) 14291;
J.L. Dormann, D. Fiorani, E. Tronc, J. Magn. Magn. Mater. 202 (1999) 251.
[30] J.-O. Andersson, C. Djurberg, T. Jonsson, P. Svedlindh, P. Nordblad, Phys. Rev. B 56 (1997) 13983.
[31] D. Kechrakos, K. Trohidou, Phys. Rev. B 58 (1998) 12169.
[32] D. Kechrakos, K.N. Trohidou, Appl. Phys. Lett. 81 (2002) 4574.
[33] S.H. Masunaga, R.F. Jardim, P.F.P. Fichtner, J. Rivas, Phys. Rev. B 80 (2009) 184428;
S.H. Masunaga, R.F. Jardim, R.S. Freitas, J. Rivas, Appl. Phys. Lett. 98 (2011) 013110.
[34] K. Nadeem, H. Krenn, T. Traussnig, R. Würschum, D. Szabó, I. Letofsky-Papst, J. Magn. Magn. Mater. 323 (2011) 1998.
[35] J. Sung Lee, R.P. Tan, J.H. Wu, Y.K. Kim, Appl. Phys. Lett. 99 (2011) 062506.
[36] P.-M. Dejardin, J. Appl. Phys. 110 (2011) 113921.
[37] B.U. Felderhof, R.B. Jones, J. Phys.: Condens. Matter 15 (2003) 4011.
[38] P.E. Jönsson, J.L. Garcıa-Palacios, M.F. Hansen, P. Nordblad, J. Mol. Liq. 114 (2004) 131.
[39] C.L. Dennis, a.J. Jackson, J.a. Borchers, R. Ivkov, a.R. Foreman, J.W. Lau, E. Goernitz, C. Gruettner, J. Appl. Phys. 103 (2008) 07A319.
[40] A. Urtizberea, E. Natividad, A. Arizaga, M. Castro, A. Mediano, J. Phys. Chem. C 114 (2010) 4916.
[41] C. Haase, U. Nowak, Phys. Rev. B 85 (2012) 045435.
[42] G.T. Landi, J. Appl. Phys. 113 (2013) 163908;
G.T. Landi, Phys. Rev. B 89 (2014) 014403.
[43] S. Ruta, R. Chantrell, O. Hovorka, Sci. Rep. 5 (2015) 9090.

[44] A. Lyberatos, R.W. Chantrell, J. Appl. Phys. 73 (1993) 6501.
[45] K. Zhang, D. Fredkin, J. Appl. Phys. 85 (1999) 5208;
K. Zhang, D.R. Fredkin, J. Appl. Phys. 87 (2000) 4795.
[46] S. Denisov, T. Lyutyy, K. Trohidou, Phys. Rev. B 67 (2003) 22.
[47] S. Titov, H. Kachkachi, Y.P. Kalmykov, W.T. Coffey, Phys. Rev. B 72 (2005) 134425.
[48] Z. Mao, D. Chen, Z. He, J. Magn. Magn. Mater. 320 (2008) 2335.
[49] D. Serantes, D. Baldomir, C. Martinez-Boubeta, K. Simeonidis, M. Angelakeris, E. Natividad, M. Castro, a. Mediano, D.-X. Chen, a. Sanchez, L. Balcells, B. Martinez, J. Appl. Phys. 108 (2010) 073918.
[50] B. Mehdaoui, R.P. Tan, A. Meffre, J. Carrey, S. Lachaize, B. Chaudret, M. Respaud, Phys. Rev. B 87 (2013) 174419;
R.P. Tan, J. Carrey, M. Respaud, Phys. Rev. B 90 (2014) 214421.
[51] E.R. Cintra, F.S. Ferreira, J.L. Santos Junior, J.C. Campello, L.M. Socolovsky, E. M. Lima, A.F. Bakuzis, Nanotechnology 20 (2009) 045103.
[52] M.A. Salvador, A.S. Costa, M. Gaeti, L.P. Mendes, E.M. Lima, A.F. Bakuzis, R. Miotto, Phys. Rev. E 93 (2006) 022609.
[53] A.F. Bakuzis, L.C. Branquinho, L. Luiz E Castro, M.T. De Amaral E Eloi, R. Miotto, Adv. Colloid Interface Sci. 191–192 (2013) 1;
L.L. Castro, G.R.R. Gonçalves, K.S. Neto, P.C. Morais, A.F. Bakuzis, R. Miotto, Phys. Rev. E 78 (2008) 061507;
M.T.A. Eloi, J.L. Santos Jr., P.C. Morais, A.F. Bakuzis, Phys. Rev. E 82 (2010) 021407.
[54] I.S. Jacobs, C.P. Bean, Phys. Rev. 100 (1955) 1060.
[55] M. Campanini, R. Ciprian, E. Bedogni, A. Mega, V. Chiesi, F. Casoli, C. de Julián Fernández, E. Rotunno, F. Rossi, A. Secchi, F. Bigi, G. Salviati, C. Magén, V. Grillo, F. Albertini, Nanoscale 7 (2015) 7717.
[56] D.F. Coral, P.M. Zélis, M. Marciello, M.D. Puerto, A. Craievich, F.H. Sanchez, M.B. F.V. Raap, Langmuir 32 (2016) 1201.
[57] T. Jonsson, J. Mattsson, P. Nordblad, P. Svedlindh, J. Magn. Magn. Mater. 168 (1997) 269.
[58] L. Néel, Ann. Géophys. 5 (1949) 99.
[59] M. El-Hilo, J. Appl. Phys. (2012), http://dx.doi.org/10.1063/1.4766817;
M. El-Hilo, R.W. Chantrell, J. Magn. Magn. Mater. 324 (2012) 2593.
[60] M.F. Hansen, P. Jönsson, P. Nordblad, P. Svedlindh, J. Phys.: Condens. Matter 14 (2002) 4901 arXiv:0010090 [cond-mat].
[61] D.V. Berkov, N.L. Gorn, J. Phys.: Condens. Matter 13 (2001) 9369.
[62] T. Jonsson, P. Nordblad, P. Svedlindh, Phys. Rev. B 57 (1998) 497.
[63] C. Djurberg, P. Svedlindh, P. Nordblad, M.F. Hansen, F. Bødker, S. Mørup, Phys. Rev. Lett. 79 (1997) 5154.
[64] P. Jönsson, T. Jonsson, J.L. Garcıa-Palacios, P. Svedlindh, J. Magn. Magn. Mater. 222 (2000) 219 arXiv:9812143 [cond-mat].
[65] B. Aslibeiki, P. Kameli, H. Salamati, M. Eshraghi, T. Tahmasebi, J. Magn. Magn. Mater. 322 (2010) 2929.
[66] B. Bittova, J. Poltierova Vejpravova, M.P. Morales, A.G. Roca, A. Mantlikova, J. Magn. Magn. Mater. 324 (2012) 1182.
[67] G.F. Goya, T.S. Berquó, F.C. Fonseca, M.P. Morales, J. Appl. Phys. 94 (2003) 3520.
[68] T. Jonsson, P. Svedlindh, M.F. Hansen, Phys. Rev. Lett. 81 (1998) 3976.
[69] W. Kleemann, O. Petracic, C. Binek, G. Kakazei, Y. Pogorelov, J. Sousa, S. Cardoso, P.P. Freitas, Phys. Rev. B 63 (2001) 1.
[70] T.C. Monson, E.L. Venturini, V. Petkov, Y. Ren, J.M. Lavin, D.L. Huber, J. Magn. Magn. Mater. 331 (2013) 156.
[71] D. Parker, V. Dupuis, F. Ladieu, J.-P. Bouchaud, E. Dubois, R. Perzynski, E. Vincent, Phys. Rev. B 77 (2008) 104428 arXiv:0802.4184.
[72] A.G. Roca, D. Carmona, N. Miguel-Sancho, O. Bomatı-Miguel, F. Balas, C. Piquer, J. Santamarıa, Nanotechnology 23 (2012) 155603.
[73] E. Winkler, R.D. Zysler, M. Vasquez Mansilla, D. Fiorani, D. Rinaldi, M. Vasilakaki, K.N. Trohidou, Nanotechnology 19 (2008) 185702.
[74] J. Zhang, C. Boyd, W. Luo, Phys. Rev. Lett. 77 (1996) 390.
[75] J.L. Dormann, L. Bessais, D. Fiorani, J. Phys. C: Solid State Phys. 21 (1988) 2015.
[76] B.R. Guduri, A.S. Luyt, J. Nanosci. Nanotechnol. 8 (2008) 2836.
[77] P. Allia, M. Coisson, P. Tiberto, F. Vinai, M. Knobel, M. Novak, W. Nunes, Phys. Rev. B 64 (2001) 144420.
[78] S. Sun, H. Zeng, D.B. Robinson, S. Raoux, P.M. Rice, S.X. Wang, G. Li, J. Am. Chem. Soc. 126 (2004) 273.
[79] M. Urban, A. Musyanovych, K. Landfester, Macromol. Chem. Phys. 210 (2009) 961.
[80] E. Snoeck, C. Gatel, L.M. Lacroix, T. Blon, J. Carrey, M. Respaud, S. Lachaize, Nano Lett. 8 (2008) 4293.